Solid Freeform Fabrication 2017: Proceedings of the 28th Annual International Solid Freeform Fabrication Symposium – An Additive Manufacturing Conference
Reviewed Paper

AN INVESTIGATION OF BUILD ORIENTATION ON SHRINKAGE IN SINTERED BIOCERAMIC PARTS FABRICATED BY VAT PHOTOPOLYMERIZATION

Donald C. Aduba, Jr.[1,2], Keyton D. Feller[3], and Christopher B. Williams[1,2]

[1]Department of Mechanical Engineering, Virginia Polytechnic Institute and State University, Blacksburg VA 24060
[2]Macromolecules Innovation Institute, Virginia Polytechnic Institute and State University, Blacksburg VA 24060
[3]Department of Chemistry, University of Wisconsin-Platteville, Platteville WI 53818

**Corresponding author
Christopher B. Williams
Virginia Polytechnic Institute and State University
College of Engineering
Design Research and Education of Additive Manufacturing Systems Laboratory
Blacksburg VA 24061
Email: cbwill@vt.edu

Abstract

In this work, a vat photopolymerization (VP) additive manufacturing process fabricated bioceramic cuboids at different build orientations to investigate their effects on post-sintering shrinkage and associated physical properties. A suspension of β-tricalcium phosphate (TCP) in Autodesk PR 57 commercial photopolymer resin and dimethyl sulfoxide (DMSO) solvent was used to shape green parts. Thermal treatment removed polymer from the green shape before sintering TCP at 1300 ˚C at 5 ˚C/min. Part morphology, dimensional shrinkage, and mass loss after sintering were evaluated. Part dimensions parallel to the build direction exhibited greater shrinkage compared to the other two dimensions. Mass loss was independent of build orientation. This paper is the first to investigate the relationship between build orientation and post-sintering shrinkage of bioceramic structures shaped by VP. In this work, an understanding of printing ceramic suspensions, and accounting for dimensional ceramic part shrinkage with respect to build orientation is gained to help guide print parameter selection to improve part fidelity and performance.

Keywords: ceramic, stereolithography, sintering, shrinkage, anisotropy, build orientation, scaffold, additive manufacturing

1. Introduction

Additive Manufacturing (AM) of bioceramics offers design freedom that enables fabricating geometrically complex structures that can be tailored for various applications in the automotive (Kaya 1999), biomedical (Cox *et al.* 2015), environmental (Nandi *et al.* 2008) and electronics (Dufaud & Corbel 2002) industries. Bioceramic materials are a major focus in the biomedical field because they mimic bone tissue with regard to osteoblast cytocompatibility, osteoconductivity, controlled biodegradability, and increased gene expression (Jones et al. 2006; Rahaman et al. 2011; Chen et al. 2006). Bioceramics can be leveraged by AM in creating complex structures captured from individual CT scans that could seamlessly integrate into the human body for bone tissue replacement. Defects affect 1,000,000 people in Europe and the United States in 2014 (Hing 2004; Parikh 2002), necessitating scaffolds with patient-specific geometric designs for seamless integration, assisting bone regeneration. AM allows for selective placement of materials in space allowing users to tailor designs to fit the specific size, shape, and porosity of the defect needed to be filled. Vat Photopolymerization (VP), also known as stereolithography™ is an AM process in which ceramic particles suspended in photocurable polymer resin is selectively cured layer by layer, to directly fabricate individualized structures without loss in material. Solidified shapes, known as green bodies are placed in a high-temperature furnace to burn out the polymer between 200-600 ˚C (Beyler & Hirschler 2002). This enables ceramic particles to diffuse into those voids left by the polymer. After polymer burnout, ceramic particles remaining join together in sintering to consolidate the green body into a fully dense ceramic structure. During consolidation, shrinkage occurs in the part may be isotropic or anisotropic, leading to reduced part quality if the original design does not account for this phenomenon. Therefore, an understanding of the ceramic part shrinkage behavior post-sintering is important to conceive optimal designs critical to successful bone tissue scaffold fabrication.

1.1 *Bioceramic printing in AM*

Bioceramics are of interest in AM due to material composition similarities to bone and dental materials, and their ability to be manufactured as complex porous scaffolds in bone implants (Osborn & Newesely 1980; Seitz *et al.* 2005). Materials such as hydroxyapatite were printed using binder jetting to create shapes with well-defined walls and inner channels down to 330 microns. Other research groups fabricated bioceramic scaffolds using robocasting deposition techniques, revealing compressive strengths and elastic moduli values similar to the bone material (Miranda *et al.* 2008). Bioceramic printing using VP requires loading a high concentration of ceramic powder (above 50% by weight) into a photopolymer resin that is selectively cured into a green body and sintered at high temperatures (**Fig. 1**) (Halloran et al. 1997). During sintering, the photocured polymer in the green body debinds between 500 and 600 ˚C, leading to the shrinkage of bioceramic parts (Scalera *et al.* 2014; Maeda *et al.* 2011). Seol *et al.* used a calcium phosphate/hydroxyapatite composite in VP to fabricate and sinter tissue engineered scaffolds. That study found a correlation between linear shrinkage of these scaffolds with respect to heating rate (Seol *et al.* 2013). Although there have been efforts to control bioceramic deposition in space using AM, there are no studies that investigate the effects of build orientation using VP on part shrinkage during sintering.

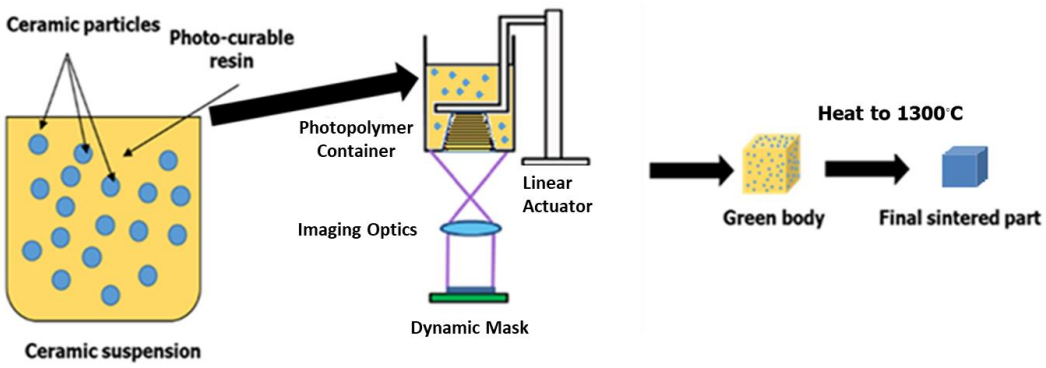

Figure 1: Schematic representation of ceramic suspension process for vat photopolymerization.

1.2 *Print orientation effects in AM*

Orientation is known to impact printed part properties in AM. Research groups have previously investigated the impact of build orientation on material properties in other areas of AM. Lee *et al.* looked at the influence of build orientation on compressive strength of parts fabricated by material extrusion and a nanocomposite deposition system, to help model their behavior (Lee *et al.* 2007). Adamczak and coauthors investigated effects of build orientation in material jetting on the ultimate tensile stress and showed there were no statistical differences (Adamczak *et al.* 2015). However, in our previous work, it was reported that orientation is known to impact printed part properties in material jetting based systems (Barclift & Williams 2012; Bass *et al.* 2016). Puebla *et al.* revealed parts built vertically using vat photopolymerization possessed significantly greater mechanical properties than parts built flat or on their edge (Puebla *et al.* 2012). More recently, research groups designed robust predictive models for dimensional shrinkage in cylindrical polymeric parts fabricated using VP. These predictive models and accompanying experimental data compensated these geometric deviations for future builds and orientations to improve dimensional accuracy (Huang *et al.* 2014; Huang *et al.* 2015). A study by Lasgorceix *et al.* evaluated shrinkage profiles of sintered ceramic structures with various porosities under different sintering temperatures (Lasgorceix et al. 2016). However, shrinkage with respect to build orientation has not been fully investigated which can better-informed print processing decisions.

1.3 *Context*

In this paper, tri-calcium phosphate (TCP) bioceramic powder (at 60% weight ratio) is blended with a commercial photopolymer resin and an organic solvent to form a photocurable suspension. This suspension is selectively cured into a green body composite and sintered to remove the polymer binders, thus creating a final densified ceramic structure. The primary focus of this paper is to investigate the shrinkage behavior of sintered bioceramic structures with respect to build orientation and their effect on physical properties. An enhanced understanding of the build orientation on the physical properties of sintered bioceramic shapes can guide the vat photopolymerization process by establishing relationships between design and build orientation selection. Build orientation selection analysis assists in the decision-making process of incorporating support structures, while accounting for the vat photopolymerization configuration and printing time.

The authors explored the influence of build orientation on dimensional shrinkage and associated physical properties of sintered TCP parts. Three build orientations were tested using a commercial bottom-up VP printer. Morphology, dimensional shrinkage, volume shrinkage, and mass loss results are presented in Section 2 of this paper. The discussion of results in Sections 3 and 4 provide important insights such as any potential correlations between build orientation and shrinkage of bioceramic parts created by vat photopolymerization. Assumptions and considerations that will have to be factored into future work are also discussed.

2. Experimental Methods

2.1 *Formulation setup*

In order to fabricate bioceramic suspensions that were selectively cured into green bodies and later sintered into dense parts, the authors selected a high solid loading ratio (60% by weight of calcium phosphate powder (0.5-10 µm size), 20% commercially available photocurable resin, and 20% organic solvent. More details of the materials used are presented in **Table 1**. After mixing the materials, the suspension was sonicated in a water bath sonicator (Omegasonics Quantum Series – 50/60 Hz) at room temperature (25 ˚C) for 10 minutes, to disperse the calcium phosphate particles. After sonication, the suspension was stirred again to recirculate particles to mitigate sedimentation before pouring into the resin vat.

Table 1. Materials for the study

Formulation component	**Amount (wt%)**	**Abbreviation**	**Supplier**
β-tricalcium phosphate (TCP)	60	TCP	Sigma-Aldrich
Black Prototyping resin (PR 57)	20	PR-57	Autodesk
Dimethyl sulfoxide (DMSO)	20	DMSO	Sigma-Aldrich

2.2 *Build orientation setup*

Autodesk Print Studio was the software used to import CAD cuboid designs with 3 mm x 6 mm x 9 mm dimensions along the X, Y and Z directions, respectively before printing. The 6 mm x 9 mm plane of the cuboid serves as a reference face to its orientation on the build platform (**Fig. 2**). The build orientation nomenclature follows ASTM standards of additively manufactured parts (ASTM International). However, for simplicity and reporting purposes, the cuboid is denoted as being oriented in the xy-plane (flat), yz-plane (edge) or zy-plane (vertical) to the build platform. (**Fig. 2**). The build direction is denoted as the z-axis.

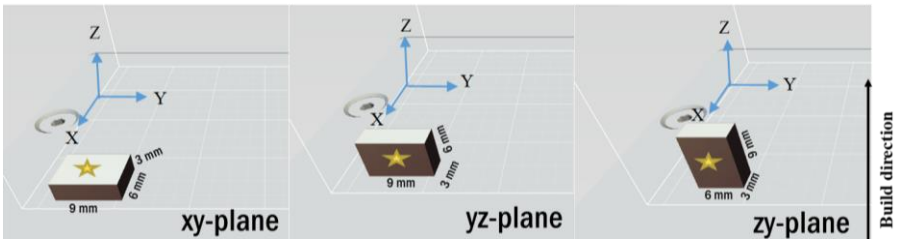

Figure 2. CAD designs of cuboids oriented on the build platform in the xy, yz, and zy-planes. The build direction occurs in the z-axis. *Denotes the reference face that is parallel to the plane of interest in the cartesian coordinate system.

2.3 *Particle size analysis*

A Horiba LA-950 laser scattering particle size analyzer measured the particle size distribution of the TCP particles to help analyze grain formation within the part morphology after sintering.

2.4 *Print process parameters*

A commercially available desktop VP printer, the Autodesk Ember with a swiper accessory kit, was used to fabricate TCP shapes from the suspension using patterned ultraviolet light from the software's slicing toolpath. The exposure time for the first layer was set to 10 seconds, to ensure that the part adhered strongly to the build platform. Subsequent model layers were cured for 2.5 seconds each based on the working curve model (**Fig. 3**) in which the cure depth and depth of penetration are 114.05 µm and critical exposure is 53.62 mJ/cm^2 respectively. It is based on the Jacobs' equation that is a linear relationship between cure depth (C_d) and light energy exposure (E) (Jacobs 1992) (**Eq. 1**). The depth of penetration (D_p) is dependent on inherent photocuring kinetics in the polymer system. This equation is used to tune exposure time for each layer in the build.

$$C_d = D_p \ln \frac{E}{E_c} \qquad \text{Eq. (1)}$$

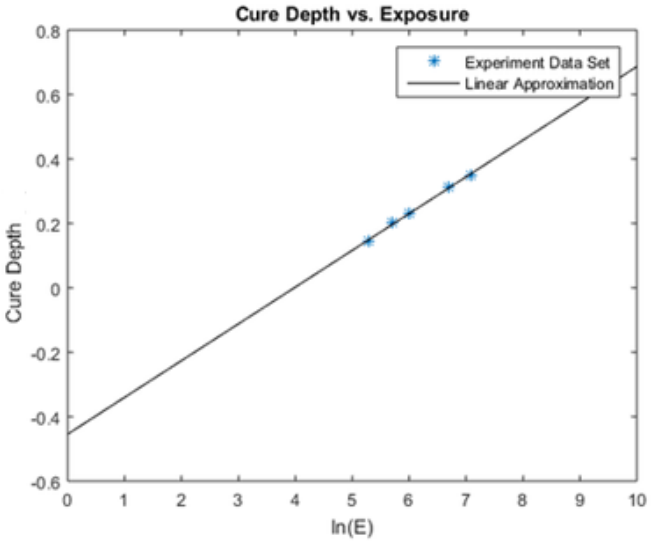

Figure 3. A semi-log plot of the working curve for TCP suspension. Energy exposure (mJ/cm^2) and Cure depth (10^{-4} m) are in the x and y-axis respectively.

After curing each layer, the resin tray was rotated 60° away from the window, to allow for the resin to re-coat the build. Subsequently, the build platform was moved up by a single layer thickness of 25 microns before the resin tray returned for curing the next layer. This process was repeated until the build was complete. The printed parts were immersed in isopropyl alcohol to remove any uncured residual monomer and blot-dried overnight before sintering.

2.5 *Sintering*

To analyze part dimensions before the sintering step, the X, Y, Z sides, and the volume of green specimens were individually measured with a digital caliper and averaged. The masses of the specimens were also recorded. In the sintering step, a programmable tube furnace purged with nitrogen was heated from room temperature at a heating rate of 5 ˚C/min to 1300 ˚C. The parts were isothermally held at 1300 ˚C for 2 h, before being cooled at a rate of 5 ˚C/min back to room temperature (**Fig. 3**), and stored before testing.

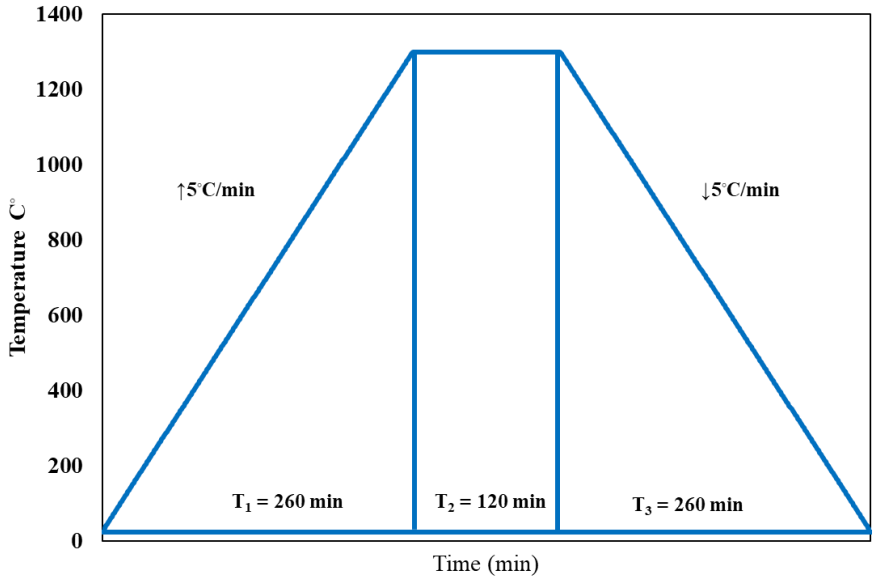

Figure 3. Sintering cycle of TCP specimens.

2.6 *Microstructural analysis*

The cross sections of fractured TCP cuboids were fixed and mounted on the surface of a 2:1 ratio mixture of EpoThin™ 2 Epoxy resin to EpoHeat™ 2 Epoxy Hardener (Buehler, Lake Bluff, IL) in a casted mould. Fixed samples are polished with a METPREP 3 polishing/grinding system to smooth fracture surfaces for morphology analysis. Polished samples were placed in an environmental SEM - FEI Quanta 600 FEG under high vacuum to analyze the cuboid grain morphology and densification after sintering.

2.7 *Dimensional shrinkage*

The X, Y and Z dimensions of sintered TCP specimens were measured with a digital caliper and averaged in an Excel spreadsheet, to determine shrinkage along each direction, and the overall volume shrinkage when compared to the green body measurements.

2.8 *Mass after sintering*

The masses of sintered TCP specimens were recorded before and after sintering, to verify if the extent of photocurable binder and solvent losses were constant across different build orientations.

2.9 *Statistical analysis*

A one-way analysis of variance (ANOVA) and an unpaired t-test were used to determine significant differences between test groups, with a significance value of $p < 0.05$.

3. Results and discussion

3.1 *Microstructural analysis*

SEM images show little difference in microstructure in fractured TCP specimens when print orientation is taken into account. For all three build orientations, voids are present in fractured samples which limit complete part consolidation after sintering. Densification may have been compromised due to omitting an isotherm in the sintering processing step designed to slowly remove organic components from the green body. As a result, voids at or below the surface appear in the sintered microstructures (**Fig. 4**). The presence of these voids compromises part flexural strength but was not reported in this study. Compromised part strength may be attributed to TCP's low material density, making it difficult to sinter into a monolithic, dense structure (Kalita et al. 2007). Incorporating more mechanically robust ceramics such as alumina and zirconia can improve mechanical strength. In the thermal treatment step, lengthening the sintering cycle to increase final bulk density or incorporating reinforcing ceramic additives such as zirconia to bridge existing voids during the sintering process will also improve strength (Wu et al. 2017). The broad particle size distribution of the feedstock powder that is consolidated into the sintered structure may also compromise strength. (**Fig. 5**) Larger particles may fuse and neck more slowly than smaller particles, leading to non-uniform grains in the consolidated structure. It is reported in traditional ceramic processes that a homogenous, finely distributed powder feedstock may improve uniform densification after sintering (Lange & Metcalf 1983; Bowen et al. 1998; Bowen & Carry 2002). Increasing the sintering time through isotherms and lower heating rates can provide more time for ceramic particles to diffuse into voids left by polymer burnout. However, larger grain boundaries would form that create longer paths for cracks to propagate within the structure (Rahimian et al. 2009).

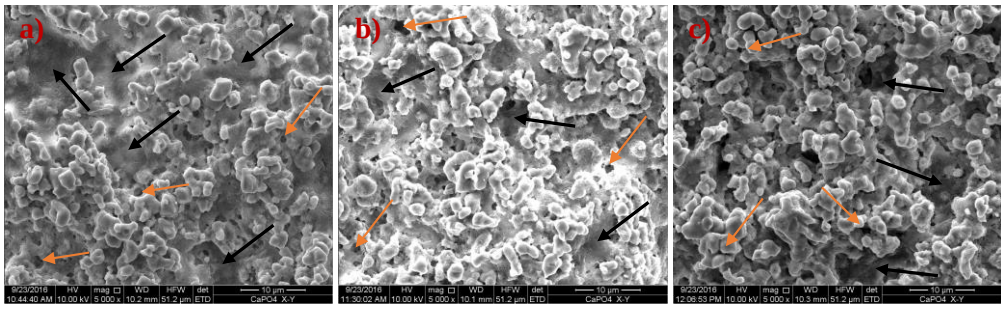

Figure 4. The bulk microstructure of TCP specimens fabricated in the **a)** x-y (Flat), **b)** y-z (Edge) and **c)** z-y (Vertical) build orientations. Black arrows denote large-scale voids beneath the fracture surface. Orange arrows denote smaller voids present at the specimen's surface. Magnification: 5000X

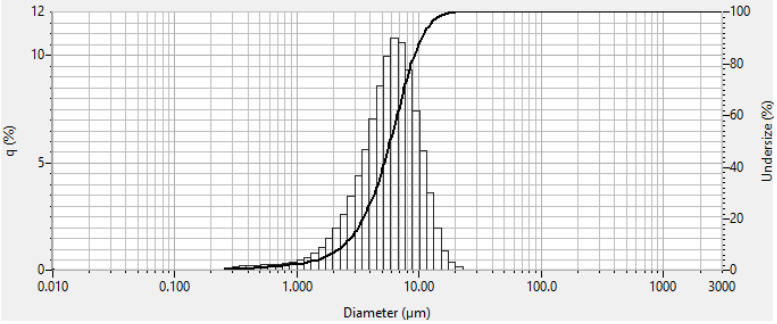

Figure 5. Particle size distribution of TCP powder feedstock used for printing. Q (%) represents percent frequency related to histogram data. Undersize (%) represents cumulative percentage of particles below the particle diameter.

3.2 *Dimensional shrinkage*

Table 2. Dimensional shrinkage of TCP cuboids with respect to the build orientation.

x-y plane (Flat)			
	Side x	**Side y**	**Side z**
Original dimensions	3 mm	6 mm	9 mm
Green body	2.98 ± 0.147 mm	6.63 ± 0.436 mm	9.64 ± 0.458 mm
Post-sintering	2.76 ± 0.091 mm	6.29 ± 0.383 mm	9.10 ± 0.453 mm
Percent shrinkage	7.14%	4.93%	5.67%
y-z plane (Edge)			
	Side x	**Side y**	**Side z**
Original dimensions	3 mm	6 mm	9 mm
Green body	3.88 ± 0.447 mm	6.00 ± 0.105 mm	9.65 ± 0.269 mm
Post-sintering	3.55 ± 0.517 mm	5.27 ± 0.253 mm	8.91 ± 0.433 mm
Percent shrinkage	8.73%	12.13%	7.74%
z-y plane (Vertical)			
	Side x	**Side y**	**Side z**
Original dimensions	3 mm	6 mm	9 mm
Green body	3.59 ± 0.296	6.49 ± 0.270	8.87 ± 0.051
Post-sintering	3.19 ± 0.402	5.93 ± 0.343	7.73 ± 0.384
Percent shrinkage	11.40%	8.66%	12.91%

Dimensional accuracies in the build orientation (i.e. sides x, y and z for x-y, y-z and z-y planes respectively) for green bodies were remarkably precise, almost matching design specifications (**Table 2**). The printer's actuator that controls the build stage in the build direction has greater resolution than the other sides and mitigates layer overcure from the solid cuboid design. Green body dimensions along the lateral directions exhibited greater values than CAD specifications deviations likely due to side scattering from TCP particles leading to layer broadening (Halloran 2016). After sintering, the dimensional shrinkage of TCP cuboids printed in the xy-plane (flat) and y-z plane (edge) was statistically greatest ($p < 0.05$) for sides in parallel to the build direction. However, TCP cuboids printed vertically (zy-plane) whose sides are parallel to the build direction did not experience statistically significant shrinkage post-sintering compared to other sides. (**Table 2**) This result could be

due to experimental error for side x measurements for both green body and post-sintered parts printed in the z-y (vertical) plane. The error is possibly attributed to TCP batch to batch processing variability which led to inconsistent final part fidelity. Additional caliper measurements along the length of individual sample cuboids are needed to improve precision in future shrinkage studies.

In summary, dimensional shrinkage values of TCP parts ranged from 4.93% to 12.91%, well within the range of linear shrinkage of bioceramics fabricated using other VP processes (Seol *et al.* 2013). The findings support that anisotropy may be present in additively manufactured parts, particularly along the build direction possibly due to ceramic settling due to gravity during the sintering step (Puebla *et al.* 2012; Lasgorceix *et al.* 2016). It could also be due to particle sedimentation during the print process resulting in mass losses biased in the build direction. Volume shrinkage was greatest in TCP cuboids printed in the zy-plane possibly due to the number of layers printed along the build direction. Here, it is hypothesized that more layers within the build printed in the zy-plane have more localized areas where polymer diffusion and shrinkage occurs during debinding and sintering.

a) **b)** **c)**

Figure 6. Layered profiles of sintered TCP parts with respect to build orientation: a) xy-plane (flat), b) yz-plane (edge) and c) zy-plane (vertical). Magnification: 46X

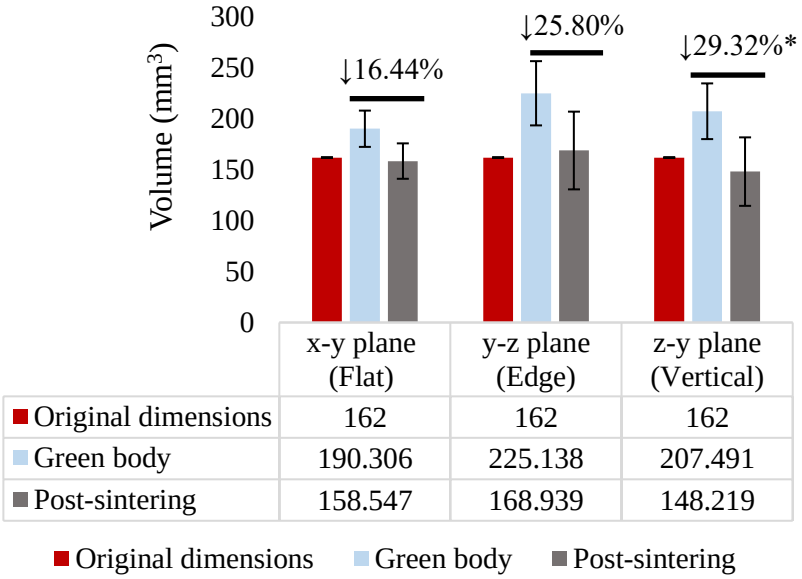

Figure 7. Volumetric shrinkages of TCP parts with respect to build orientation. (*denotes statistical significance at $p < 0.05$)

3.3 *Mass loss after sintering*

Mass loss of the sintered parts reveals it is independent of build orientation and shrinkage anisotropy. (**Fig. 8)** A one-way ANOVA statistical analysis showed no significant differences in the mass loss with respect to build orientation. According to mass loss data, the photocurable binder and solvent were removed in the sintering cycle because organic compounds thermally degrade at temperatures above 200 ˚C (Beyler & Hirschler 2002). The mass loss values ranged from 46.20 to 49.42 percent which is more than the expected mass loss (40%). This phenomenon may be due to particle sedimentation, leading to fewer particles at the resin surface for printing. This problem is likely caused by low viscosity (1.9 cPs) properties of DMSO solvent and predominantly micron sized TCP powders in the suspension (LeBel & Goring 1962). DMSO solvent viscosity promotes low surface tension yielding small resistance forces to oppose particle sedimentation Incorporating charged or long-chain polymer dispersants with higher viscosity minimize particle agglomeration and help minimize sedimentation in the ceramic suspension (Lange 1989; Lewis 2004).

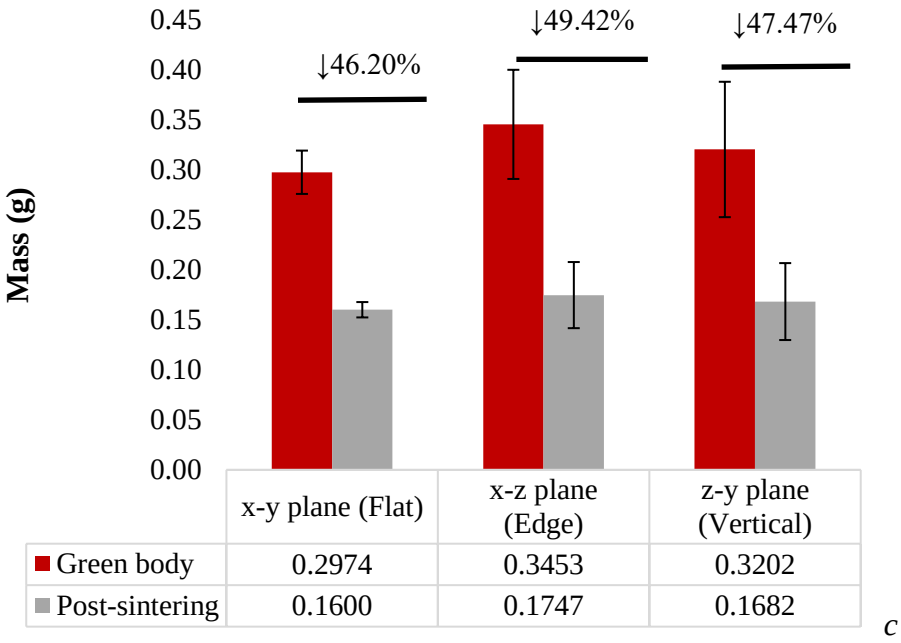

c

Figure 8. Mass loss in TCP cuboid specimens with respect to build orientation after sintering.

3.4 *Summary of Key Findings*

The authors evaluated dimensional shrinkage of sintered TCP cuboids printed using vat photopolymerization to determine if it is influenced by the part build orientation. This investigation concluded that:

- Cuboids printed in the zy-plane (vertical orientation) exhibit statistically significant greater volume shrinkage values than the other two build orientations, possibly due to greater interlayer junctions prone to shrinkage during sintering.

- In cuboids that were printed in the xy (flat) and yz-planes (edge), the side that is parallel to the build direction exhibit statistically significant greater shrinkage than the other two sides. This was not significant for parts printed in the zy-plane (vertical).
- TCP mass loss in sintered cuboids does not demonstrate statistical agreement with build orientation.
- TCP cuboid cross-sectional morphology possesses voids that limit full densification.
- More consistent batch to batch processing is needed to reduce measurement variability in green and sintered parts.
- Testing a wider range of ceramics with different material properties is necessary to validate the aforementioned phenomena.
- Biocompatibility assessment of TCP and other bioceramics printed by VP should be investigated for tissue engineering applications.
- Analyzing more microstructural properties such as crystalline order, structure, interlayer bonding, defects, and orientation of bioceramics materials printed by VP and how they change with respect to directional shrinkage is critical to making reproducible printed parts.

4. Conclusion

In this work, three-dimensional β-tricalcium phosphate builds from photocurable suspension was demonstrated using a vat photopolymerization additive manufacturing process. Preliminary work on dimensional and volume shrinkage of scalene cuboids with respect to build orientation suggests orientations with greater build layers lead to greater shrinkage. Dimensional shrinkage results suggest that the dimension parallel to the build direction exhibits the greatest shrinkage compared to the other two sides. Findings from this paper warrant further investigation in ceramic particle process control to create more detailed models to compensate expected shrinkage behavior.

Understanding anisotropic shrinkage behavior in additively manufactured bioceramics has the potential to reliably create functional tissue engineering scaffolds with the ability to provide mechanical support and biological cues for tissue growth (**Fig. 9**).

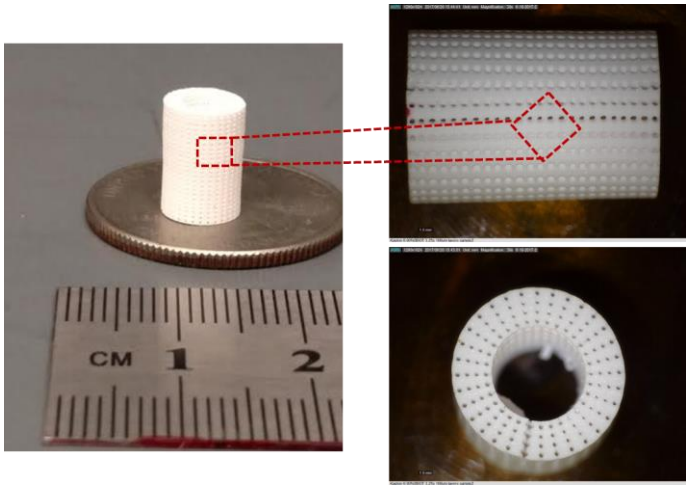

Figure 9. A sintered porous alumina bioceramic cylindrical scaffold under light microscopy. 30X Magnification

Improvement of suspension processing, printing and sintering are necessary to gain more reliable analysis of the ceramic structures. In future studies, particle sedimentation within the resin vat should be quantitatively measured to determine downstream effects on part strength and material homogeneity. An evaluation of the sintering process, specifically control across different sintering temperatures and rates are needed to give insight on affecting dimensional shrinkage, and whether it is influenced by build orientation. Computational physics-based modeling techniques should be employed in future studies to examine particle interactions at discrete levels, to simulate shrinkage across the part. At a machine level, the configuration of projected or scanned ultraviolet light source in the vat photopolymerization setup may influence build orientation selection among other design considerations outlined in our previous work (Lambert et al. 2013). Vat Photopolymerization of bioceramics enables fabrication of high-resolution, biocompatible parts designed to potentially function as bone tissue scaffold models. This paper aims to provide a perspective using this Additive Manufacturing process and thermal post-processing conditions to assess and improve the final geometric fidelity of these class of three-dimensional materials.

5. Acknowledgments

This project was supported by funding from RJ Reynolds, Winston-Salem, North Carolina, USA. K.F. thanks the National Science Foundation Research Experience for Undergraduates (REU) program from the Division of Chemistry (CHE-1560240). The authors would like to thank Dr. Tom Staley and Hesham Elmkharram in the Materials Science and Engineering Department at Virginia Tech for providing access to their furnace facilities. Authors thank Steve McCartney at the Nanoscale Characterization and Fabrication Laboratory (NCFL) for assistance with SEM images. D.A. thanks Dr. Susheel Sekhar for proofreading the manuscript and providing CAD designs for printing.

References:

Adamczak, S., Bochnia, J. & Kaczmarska, B., 2015. METROLOGY AND MEASUREMENT SYSTEMS AN ANALYSIS OF TENSILE TEST RESULTS TO ASSESS THE INNOVATION RISK FOR AN ADDITIVE MANUFACTURING TECHNOLOGY. *Metrol. Meas. Syst*, XXII(1), pp.127–138. Available at: www.metrology.pg.gda.pl [Accessed August 30, 2016].

ASTM International, Standard Practice for Reporting Data for Test Specimens Prepared by Additive Manufacturing 1.

Barclift, M.W. & Williams, C.B., 2012. EXAMINING VARIABILITY IN THE MECHANICAL PROPERTIES OF PARTS MANUFACTURED VIA POLYJET DIRECT 3D PRINTING. In *International Solid Freeform Fabrication Symposium*. pp. 876–890.

Bass, L.B., Meisel, N.A. & Williams, C.B., 2016. Exploring variability in material properties of multi-material jetting parts. *Rapid Prototyping Journal*, 22(5).

Beyler, C.L. & Hirschler, M.M., 2002. Thermal Decomposition of Polymers. *SFPE handbook of fire protection engineering*, 2(32). Available at: http://ewp.rpi.edu/hartford/~ernesto/F2012/EP/MaterialsforStudents/Patel/Beyler_Hirschler_SFPE_Handbook_3.pdf [Accessed March 7, 2017].

Bowen, P. et al., 1998. Processing of Nanosized Ceramic Powders -- A Bimodal Slip Casting Approach. *Ceramic Transactions*, pp.211–218. Available at: https://www.tib.eu/en/search/id/BLCP%3ACN028617442/Processing-of-Nanosized-Ceramic-Powders-A-Bimodal/?tx_tibsearch_search%5Bsearchspace%5D=tn [Accessed March 11, 2017].

Bowen, P. & Carry, C., 2002. From powders to sintered pieces: forming, transformations and sintering of nanostructured ceramic oxides. *Powder Technology*, 128(2–3), pp.248–255. Available at: http://linkinghub.elsevier.com/retrieve/pii/S0032591002001833 [Accessed March 11, 2017].

Chen, Q.Z., Thompson, I.D. & Boccaccini, A.R., 2006. 45S5 Bioglass-derived glass-ceramic scaffolds for bone tissue engineering. *Biomaterials*, 27(11), pp.2414–2425. Available at: http://linkinghub.elsevier.com/retrieve/pii/S0142961205010422 [Accessed June 15, 2017].

Cox, S.C. et al., 2015. 3D printing of porous hydroxyapatite scaffolds intended for use in bone tissue engineering applications. *Materials science & engineering. C, Materials for biological applications*, 47, pp.237–47. Available at: http://www.sciencedirect.com/science/article/pii/S0928493114007255 [Accessed May 9, 2016].

Dufaud, O. & Corbel, S., 2002. Stereolithography of PZT ceramic suspensions. *Rapid Prototyping Journal*, 8(2), pp.83–90.

Halloran, J., Griffith, M. & Chu, T.-M., 1997. Stereolithography resin for rapid prototyping of ceramics and metals.

Halloran, J.W., 2016. Ceramic Stereolithography: Additive Manufacturing for Ceramics by Photopolymerization. *Annu. Rev. Mater. Res.*, 46, pp.19–40.

Hing, K.A., 2004. Bone repair in the twenty–first century: biology, chemistry or engineering? *Philosophical Transactions of the Royal Society of London A: Mathematical, Physical and Engineering Sciences*, 362(1825). Available at: http://rsta.royalsocietypublishing.org/content/362/1825/2821.long [Accessed June 15, 2017].

Huang, Q. et al., 2015. Optimal offline compensation of shape shrinkage for three-dimensional printing processes. *IIE Transactions*, 47, pp.431–441.

Huang, Q. et al., 2014. Predictive modeling of geometric deviations of 3D printed products - A unified modeling approach for cylindrical and polygon shapes. In *2014 IEEE International Conference on Automation Science and Engineering (CASE)*. IEEE, pp. 25–30. Available at: http://ieeexplore.ieee.org/lpdocs/epic03/wrapper.htm?arnumber=6899299 [Accessed August 31,

2016].
Jacobs, P.F., 1992. *Rapid prototyping & manufacturing: fundamentals of stereolithography.*, Society of Manufacturing Engineers.
Jones, J.R., Ehrenfried, L.M. & Hench, L.L., 2006. Optimising bioactive glass scaffolds for bone tissue engineering. *Biomaterials*, 27(7), pp.964–973. Available at: http://linkinghub.elsevier.com/retrieve/pii/S0142961205006319 [Accessed June 15, 2017].
Kalita, S.J., Bhardwaj, A. & Bhatt, H.A., 2007. Nanocrystalline calcium phosphate ceramics in biomedical engineering. *Materials science & engineering. C,*, 27, pp.441–449.
Kaya, H., 1999. The application of ceramic-matrix composites to the automotive ceramic gas turbine. *Composites Science and Technology*, 59(6), pp.861–872.
Lambert, P.M., Campaigne III, E.A. & Williams, C.B., 2013. DESIGN CONSIDERATIONS FOR MASK PROJECTION MICROSTEREOLITHOGRAPHY SYSTEMS. *Solid Freeform Fabrication Conf.*
Lange, F.F., 1989. Powder Processing Science and Technology for Increased Reliability. *Journal of the American Ceramic Society*, 72(1), pp.3–15. Available at: http://doi.wiley.com/10.1111/j.1151-2916.1989.tb05945.x [Accessed February 21, 2017].
Lange, F.F. & Metcalf, M., 1983. Processing-Related Fracture Origins: II, Agglomerate Motion and Cracklike Internal Surfaces Caused by Differential Sintering. *Journal of the American Ceramic Society*, 66(6), pp.398–406. Available at: http://doi.wiley.com/10.1111/j.1151-2916.1983.tb10069.x [Accessed March 11, 2017].
Lasgorceix, M., Champion, E. & Chartier, T., 2016. Shaping by microstereolithography and sintering of macro–micro-porous silicon substituted hydroxyapatite. *Journal of the European Ceramic Society*, 36(4), pp.1091–1101. Available at: http://linkinghub.elsevier.com/retrieve/pii/S0955221915302314 [Accessed February 27, 2017].
LeBel, R.G. & Goring, D.A.I., 1962. Density, Viscosity, Refractive Index, and Hygroscopicity of Mixtures of Water and Dimethyl Sulfoxide. *Journal of Chemical & Engineering Data*, 7(1), pp.100–101. Available at: http://pubs.acs.org/doi/abs/10.1021/je60012a032 [Accessed June 25, 2017].
Lee, C.S. et al., 2007. Measurement of anisotropic compressive strength of rapid prototyping parts. *Journal of Materials Processing Technology*, 187, pp.627–630.
Lewis, J.A., 2004. Colloidal Processing of Ceramics. *Journal of the American Ceramic Society*, 83(10), pp.2341–2359. Available at: http://doi.wiley.com/10.1111/j.1151-2916.2000.tb01560.x [Accessed June 25, 2016].
Maeda, C., Tasaki, S. & Kirihara, S., 2011. Accurate Fabrication of Hydroxyapatite Bone Models with Porous Scaffold Structures by Using Stereolithography. *IOP Conf. Series: Materials Science and Engineering*, 18, pp.1–4. Available at: http://iopscience.iop.org/1757-899X/18/7/072017 [Accessed June 24, 2016].
Miranda, P. et al., 2008. Mechanical properties of calcium phosphate scaffolds fabricated by robocasting. *Journal of Biomedical Materials Research Part A*, 85A(1), pp.218–227. Available at: http://doi.wiley.com/10.1002/jbm.a.31587 [Accessed August 31, 2016].
Nandi, B.K., Uppaluri, R. & Purkait, M.K., 2008. Preparation and characterization of low cost ceramic membranes for micro-filtration applications. *Applied Clay Science*, 42(1), pp.102–110.
Osborn, J.F. & Newesely, H., 1980. The material science of calcium phosphate ceramics. *Biomaterials*, 1(2), pp.108–111. Available at: http://linkinghub.elsevier.com/retrieve/pii/0142961280900095 [Accessed September 1, 2016].
Parikh, S.N., 2002. Bone Graft Substitutes in Modern Orthopedics. *Orthopedics*, 25(11), pp.1301–

1309. Available at: https://www.healio.com/orthopedics/journals/ortho/2002-11-25-11/%7B8325a759-4d03-443b-b393-3667c2b901d6%7D/bone-graft-substitutes-in-modern-orthopedics [Accessed June 15, 2017].

Puebla, K. et al., 2012. Effects of environmental conditions, aging, and build orientations on the mechanical properties of ASTM type I specimens manufactured via stereolithography. *Rapid Prototyping Journal*, 18(5), pp.374–388. Available at: http://www.emeraldinsight.com/doi/abs/10.1108/13552541211250373 [Accessed August 30, 2016].

Rahaman, M.N. et al., 2011. Bioactive glass in tissue engineering. *Acta Biomaterialia*, 7(6), pp.2355–2373. Available at: http://linkinghub.elsevier.com/retrieve/pii/S1742706111001280 [Accessed June 15, 2017].

Rahimian, M. et al., 2009. The effect of particle size, sintering temperature and sintering time on the properties of Al–Al2O3 composites, made by powder metallurgy. *Journal of Materials Processing Technology*, 209(14), pp.5387–5393.

Scalera, F. et al., 2014. Development and characterization of UV curable epoxy/hydroxyapatite suspensions for stereolithography applied to bone tissue engineering. *Ceramics International*, 40(10), pp.15455–15462.

Seitz, H. et al., 2005. Three-dimensional printing of porous ceramic scaffolds for bone tissue engineering. *Journal of Biomedical Materials Research Part B: Applied Biomaterials*, 74B(2), pp.782–788. Available at: http://doi.wiley.com/10.1002/jbm.b.30291 [Accessed August 31, 2016].

Seol, Y.-J. et al., 2013. A new method of fabricating robust freeform 3D ceramic scaffolds for bone tissue regeneration. *Biotechnology and Bioengineering*, 110(5), pp.1444–1455. Available at: http://doi.wiley.com/10.1002/bit.24794 [Accessed August 17, 2016].

Wu, H. et al., 2017. Fabrication of dense zirconia-toughened alumina ceramics through a stereolithography-based additive manufacturing. *Ceramics International*, 43.1, pp.968–972.